Fluorescent core–shell silica nanoparticles: towards "Lab on a Particle" architectures for nanobiotechnology

Andrew Burns,[a] Hooisweng Ow[b] and Ulrich Wiesner*[a]

Received 31st July 2006
First published as an Advance Article on the web 15th September 2006
DOI: 10.1039/b600562b

Novel nanoscale fluorescent materials are integral to the progress of emergent fields such as nanobiotechnology and facilitate new research in a variety of contexts. Sol–gel derived silica is an excellent host material for creating fluorescent nanoparticles by the inclusion of covalently-bound organic dyes. Significant enhancements in the brightness and stability of organic dye emission can be achieved for silica-based core–shell nanoparticle architectures at length scales down to tens of nanometers with narrow size distributions. This *tutorial review* will highlight these findings and describe the evolution of the fluorescent core–shell silica nanoparticle concept towards integration of multiple functionalities including mesoporosity, metal nanoshells and quantitative chemical sensing. These developments point towards the development of "lab on a particle" architectures with promising prospects for nanobiotechnology, drug development and beyond.

Introduction

In this review, recent progress in the field of core–shell fluorescent silica nanomaterials will be described, with special emphasis on applications in the emerging field of nanobiotechnology. Rather than attempting a general overview of this exciting and rapidly growing research field, general features, challenges and future trends will be highlighted through examples of the recent work of the Wiesner group and collaborators at Cornell University. This work encompasses water-soluble, non-toxic fluorescent core–shell silica nanoparticles of various compositions and architectures with unusually high brightness and photostability levels, as well as narrow particle size distributions suited for applications in the life sciences and beyond, as illustrated in Fig. 1.

The review will begin with an introduction to nanoscale fluorescent materials, focusing on the materials issues central to creating effective emitters, including a brief review of several common classes of photoemitters. We will then introduce fluorescent core–shell silica nanoparticles as a materials platform, focusing on their photophysical and materials characterization. The versatility of the silica-based particle synthesis will be demonstrated through control of specific particle characteristics such as color and size, as well as through the integration of novel particle properties such as mesoporosity or metal shells. Further, we will cover two applications of specific core–shell silica nanoparticle architectures in nanobiotechnology, emphasizing the integration of two different functionalities to create effective probes of biology on the nanoscale. Finally, we will begin to explore some of the possibilities for future research, building on the

[a]*Dept. of Materials Science & Engineering, Cornell University, Ithaca, NY 14853, USA. E-mail: ubw1@cornell.edu; Fax: (607)-255-2365*
[b]*Hybrid Silica Technologies, Ithaca, NY 14850, USA*

Andrew Burns

Andrew Burns was born on Long Island, NY in 1981. He completed an undergraduate degree in Chemistry at the University of Delaware where he performed research on photocatalytic nanomaterials in the group of Prof. S. Ismat Shah in Materials Science & Engineering. He is currently a PhD candidate in Materials Science & Engineering at Cornell University working in the group of Prof. Ulrich Wiesner on the development of fluorescent silica nanoparticles for imaging, sensing and understanding biology at small length scales.

Hooisweng Ow

Hooisweng Ow was born in Batu Pahat, Malaysia. She completed an undergraduate degree in Ceramic Engineering at Alfred University in upstate New York where she did collaborative research with the Pacific Northwest National Laboratory on the ionic conductivity of cathode materials for solid oxide fuel cells. She then completed a PhD in Materials Science & Engineering at Cornell University in the group of Prof. Ulrich Wiesner where she developed a class of fluorescent core–shell silica nanoparticles. She is currently continuing her work in hybrid nanoscale materials as Chief Technologist at Hybrid Silica Technologies, Inc. in Ithaca, NY.

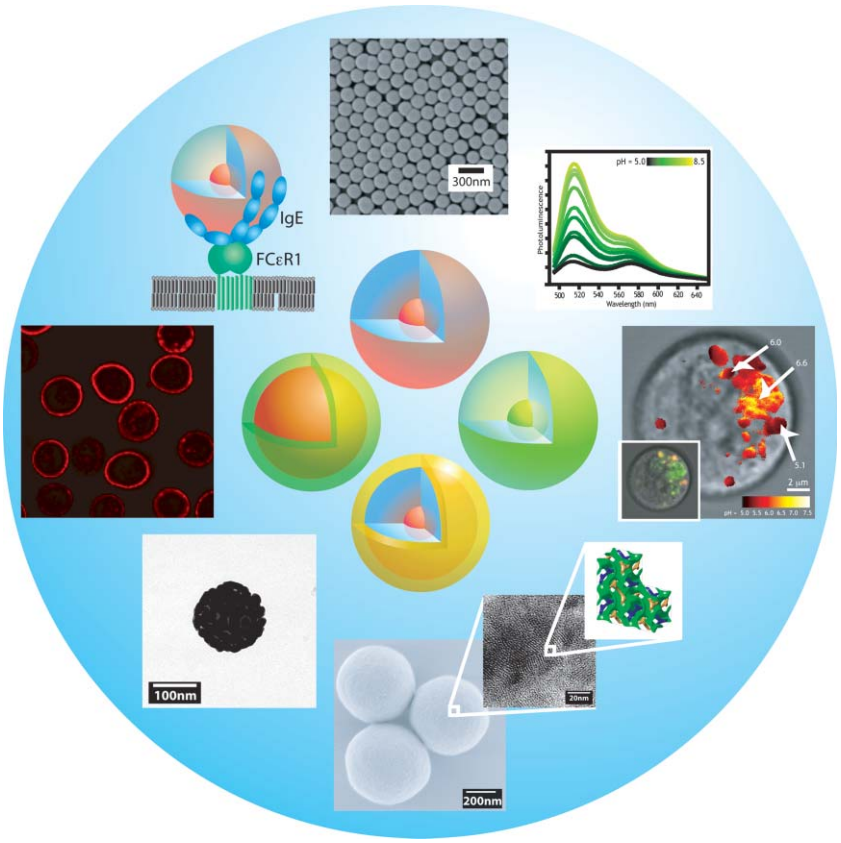

Fig. 1 An overview of the versatility of the fluorescent core–shell silica nanoparticle platform: illustrations of single and dual-emission particles as well as gold-nanoshell encapsulated core–shell particles are shown at the heart of the figure, while a variety of applications including bioimaging, drug delivery, sensing and therapeutics are shown in the periphery.

versatility of silica as a host material and the modularity of the core–shell architecture to build highly integrated "lab on a particle" architectures (LPs).

1. Fluorescent nanoscale materials

The phenomenon of fluorescence is ubiquitous in fields from biology to information technology and beyond. The excellent spatial (diffraction limit or better) and temporal (nanosecond) resolution, as well as the high signal-to-noise ratios inherent to fluorescent analyses, make fluorescent materials ideally suited to the exploration of the nanoscale. The development of novel fluorescent materials is integral to the progress of emergent fields such as nanobiotechnology, photonics and optoelectronics. Every application has its own particular constraints, but the fundamental issues for any fluorescent material are the same: brightness and stability. There are several classes of materials that are currently employed as fluorescent emitters/probes, including organic and metallorganic dye molecules, fluorescent proteins, semiconductor quantum dots, polymer/dye-based nanoparticles and silica/dye hybrid particles (Fig. 2), each with their own advantages and disadvantages as recently reviewed by Wang *et al.*[1]

Ulrich Wiesner

Ulrich Wiesner studied Chemistry in Mainz, Germany, and Irvine, California. He gained his PhD in 1991 with work at the Max-Planck-Institute for Polymer Research (MPI-P), Mainz, and was a postdoctoral fellow at the E.S.P.C.I. in Paris, France until 1993. He joined the Cornell MS&E faculty in 1999 following his Habilitation and became a Full Professor in 2005. He works at the interface between polymer science and solid state chemistry/physics with the goal of generating novel hierarchical and multifunctional hybrid materials. He is the co-founder of Hybrid Silica Technologies, Inc. and the recipient of multiple awards including the Carl Duisberg Memorial Award of the German Chemical Society.

1.1 Organic and metallorganic dye molecules

The smallest (and generally dimmest) fluorescent emitters in use today are single organic or metallorganic dye molecules, which generally consist of π-conjugated ring structures such as xanthenes, pyrenes or cyanines.[2] These fluorophores are commercially available with emissions across the spectrum from UV to the near infrared (~300–900 nm) and may be fine-tuned to particular wavelengths or applications by changing the chemistry of their substituent groups. As shown in Fig. 2a, the small size of individual dye molecules (~1 nm) make them an excellent choice for many applications, especially in biology

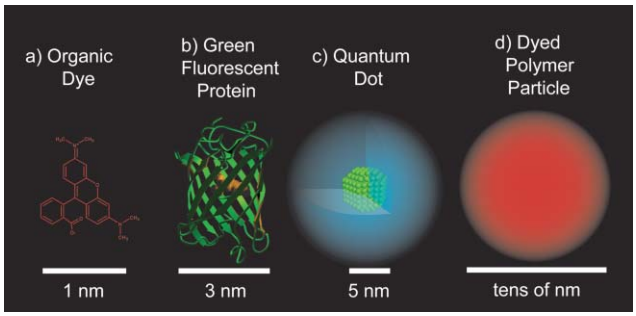

Fig. 2 Several common fluorescent nanoscale materials including (a) organic dye molecules (tetramethylrhodamine), (b) green fluorescent protein, (c) polymer-coated, water soluble semiconductor quantum dots and (d) dyed polymer particles.

where researchers seek to minimize the physical perturbations to the system under investigation. However, small size can also be detrimental, leading to non-specific labeling and high background signals as dyes diffuse away from their intended targets. Spectrally, organic dyes tend to have fairly wide absorption and emission spectra (FWHM $\sim$ 50 nm), which can lead to spectral overlap and re-absorption when using multiple dye species simultaneously.[3] In normal use, dye molecules are exposed to a variety of harsh environments and often suffer from photobleaching and quenching due to interactions with solvent molecules and reactive species such as oxygen or ions dissolved in solution. Further, the lack of protection manifests itself in the π–π stacking behavior that many dyes exhibit at high local concentrations, *e.g.* when deposited on surfaces or interfaces, leading to energy transfer and dye quenching.[4] The fluorescent and chemical properties of these single molecule fluorophores are detailed in texts by Haugland[2] and Lakowicz[3] and were recently reviewed by Wang *et al.*[1]

1.2 Fluorescent proteins

Increasing in size from single dye molecules, green fluorescent proteins (GFP), such as those originally isolated from Aequora jellyfish (Fig. 2b), are of great interest to biologists for their ability to indicate genetic expression levels in living systems by the addition of the GFP sequence genes to the host's genome (reviewed by Wang[1] and Tsien[5]). A variety of related fluorescent proteins have been generated, covering much of the visible spectrum, permitting simultaneous labeling of multiple genetic activities within the same system. Although their fluorescence emission is similar to organic dyes, fluorescent proteins are fundamentally different from other labels, as their synthesis and localization are dependent primarily upon the gene transcription activity of the host cell or organism, rather than any external targeting. Similar to dyes, the fluorescent proteins tend to exhibit excited state interactions which can lead to stochastic blinking, quenching and photobleaching.[5]

1.3 Semiconductor quantum dots

Colloidal semiconductor quantum dots (QDs) were among the first nanomaterials to attract the attention of the biological community. These nanoparticles (hundreds to thousands of atoms) are traditionally made from crystals of II–VI or III–V elements (PbS, CdSe, *etc.*) or other semiconductors and may be synthesized in many different colors by tuning the particle size (2–50 nm) to change the Bohr exciton radius, and thus the wavelength of the emitted light (Fig. 2c). QDs exhibit fundamentally different absorption and emission behavior from dyes and fluorescent proteins, characterized by wide absorptions with large absorption cross-sections (10–100$\times$ dye), large Stokes' shifts, narrow emission bands (FWHM $\sim$20–40 nm) and minimal photobleaching.[6]

Most QDs are hydrophobic by nature, requiring layers of polymeric or inorganic material to compatiblize them with the aqueous conditions of biology and other fields, increasing their effective hydrodynamic radii to 15 nm or more. Additionally, QDs are generally made from heavy metal ions such as Pb^{2+} or Cd^{2+}, so their use exposes researchers and experimental systems to these toxic materials as well as generating a toxic waste stream into the environment.[7] In addition to the stochastic blinking phenomena seen in all single emitter systems, recent work has shown that more than 40% of quantum dots used under biological conditions may exhibit dark states,[8] requiring the use of higher labeling concentrations to yield the desired brightness. The biological applications and photophysical properties of quantum dots were recently detailed in reviews by Mattoussi[6] and Parak.[9]

1.4 Dyed polymer nanoparticles

Another common class of fluorescent materials is based on polymers such as dextran or polystrene latex beads in combination with organic dyes (Fig. 2d). These approaches generally incorporate the dye by covalent attachment of the dye molecules to the polymer chain or physical entrapment in a cross-linked particle.[1,2] This often leads to low incorporation rates and offers little protection to the dye molecules, making these probes prone to leaching, quenching and photobleaching interactions under working conditions.

1.5 Fluorescent silica nanoparticles

In order to create more robust emitters, researchers have developed hybrid organic/inorganic nanoparticles from organic dye molecules and amorphous silica. As a matrix material for fluorescent probes, silica provides a chemically and mechanically stable vehicle, which can protect the encapsulated dye molecules from external perturbations, while exposing a biocompatible and easily functionalized surface to the environment and in some cases enhancing the photophysical properties of the encapsulated dyes.[10]

Spherical silica nanoparticles are generally made by one of two chemical approaches: reverse microemulsion or sol–gel synthesis. Reverse microemulsion techniques rely on the controlled aqueous environment within surfactant-confined micelles in a non-polar solvent to create monodisperse spherical colloids. Such nanoparticle syntheses were extensively explored by Arriagada and Osseo-Asare[11] in the 1990s, and are continued today by the Tan group that began developing fluorescent nanoparticles in the mid-1990s by physically entrapping metallorganic dyes such as

tris(2,2′-bipyridyl)dichlororuthenium in silica nanoparticles.[12] The confined ''nanoreactor'' environment within the reverse micelle has been shown to yield highly monodisperse particles and increase the incorporation of nonpolar molecules, which are often difficult to incorporate into the hydrophilic silica matrix. However, the lack of covalent attachment of the fluorophore to the silica matrix means that the dye molecules can leach out of the particles over time, decreasing per-particle brightness, increasing background signal and exposing the dyes to their environment. Further, these syntheses often have low yields and the use of surfactants necessitates extensive washing to remove the surfactant molecules before any biological application to avoid disruption or lysis of biomembranes by the surfactant molecules.

Alternatively, in the late 1960s, Stöber and co-workers developed a mild synthetic protocol for growing monodisperse spherical silica nanoparticles ($\sim$100 nm) based on the sol–gel chemistry of silicon alkoxides.[13] Stöber's method involves the hydrolysis and condensation of tetraethoxysilane (TEOS) in ethanol solution in the presence of water with ammonia as a catalyst to create monodisperse, spherical, electrostatically-stabilized particles. The Stöber synthesis was investigated by several groups to determine the effects of the various reagents on size, reaction kinetics, monodispersity and sphericity of the particles.[14] The van Blaaderen group expanded on this work by covalently incorporating organic fluorophores into the silica matrix by coupling them to reactive organosilicates.[15] Throughout this work, the particle sizes reported remained in the hundreds of nanometers to microns regime, which are useful for many applications such as the study of colloid dynamics and photonic crystals, but are generally too large to be truly effective probes for biology.

2. Bright and stable fluorescent core–shell silica nanoparticles: C dots

In 2005, we reported the synthesis of organic dye/silica-based core–shell nanoparticles referred to as C dots, with hydrodynamic radii on the order of 10–15 nm and per-particle brightness levels approaching those of quantum dots.[10] Size control and brightness are achieved by encapsulating the emitters within the core of a core–shell nanoparticle (Fig. 3a). Towards this end, we have built upon the work of the van Blaaderen group to develop fluorescent silica precursors by the coupling of a reactive dye species with an organosilicate source. The hybrid precursors are then hydrolyzed and condensed with pure silica to yield hybrid organic/inorganic cores. These cores act as heterogeneous nuclei for the growth of a pure silica shell, further protecting the encapsulated dyes. This concept was originally demonstrated by incorporating multiple tetramethylrhodamine isothiocyanate (TRITC) dye molecules into uniform, monodisperse, 25 nm diameter core–shell particles (Fig. 3b).[10]

2.1 Photophysical characterization

The photophysical properties of these core–shell particles and their constituent parts were further characterized to determine, *e.g.*, the effects of encapsulation on dye brightness and

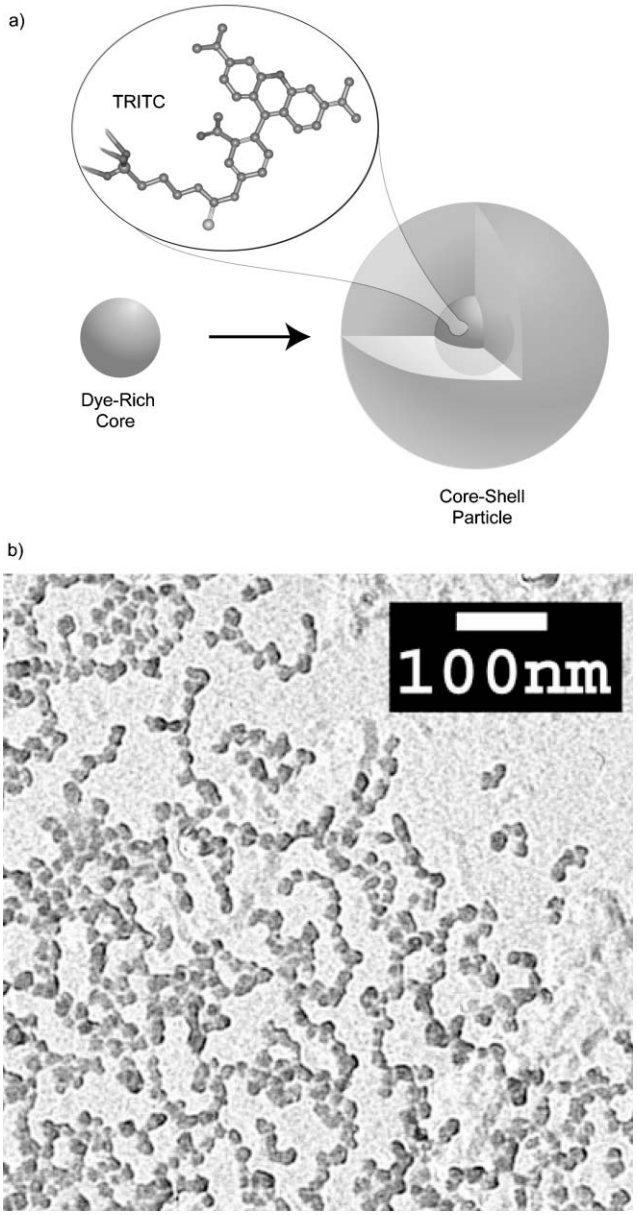

Fig. 3 (a) A schematic representation of the dye-rich core–shell architecture of the C dot particles, in this case covalently incorporating the organic dye tetramethylrhodamine isothiocyanate (TRITC) and (b) a representative TEM image of 30 nm diameter TRITC-based core–shell silica nanoparticles with a narrow particle size distribution. (Reproduced, in part, with permission from *Nano Lett.*, 2005, **5**, 113–117.[10] Copyright 2005 American Chemical Society.)

stability. In order to probe the behavior of single particles, multi-photon fluorescence correlation spectroscopy (FCS) was employed.[16] This technique is similar to dynamic light scattering (DLS) except that the detected light used for analysis is from fluorescence, rather than scattering. From the autocorrelation of the time-domain signal, the diffusion coefficient of the emitters can be determined, giving the particle size *via* the Stokes–Einstein equation. The signal intensity scales with the number of emitters within the multi-photon focal volume ($\sim$100 attoliters[17]) resulting in very accurate concentration information that can be employed to

determine per-particle brightness for each of the diffusing species. Finally, analysis of the accuracy of the fit to the FCS autocorrelation decay curves gives a precise measure of the particle size distribution.[16,18]

First, FCS measurements were made on a series of the parent fluorophores, cores, and core–shell particles made from a single synthesis. The TRITC dye molecules were found to have hydrodynamic radii of approximately 1.0 nm, while the core particles were found to be 2.2 nm in radius, and the final core–shell particles were 15 nm in radius (Fig. 4a) with a narrow particle size distribution. Interestingly, it was found that although containing multiple fluorophores, the per-particle brightness of the cores was less than that of both the core–shell particles and the free dye molecules, suggesting mutual quenching of the dyes (Fig. 4b). Fig. 4 further demonstrates that the addition of the silica shell onto the core significantly enhances the brightness of the core–shell particles. Fluorescence lifetime measurements show that this phenomenon can be attributed to an increase in the radiative and a decrease in the non-radiative decay rates for the dyes upon encapsulation in the core–shell architecture leading to an enhanced dye quantum yield.[19] Further, rotational anisotropy measurements show that the decrease in the non-radiative decay rate correlates well with the rigidity of the dye environment in the silica particle as compared to the free dye in solution.[19]

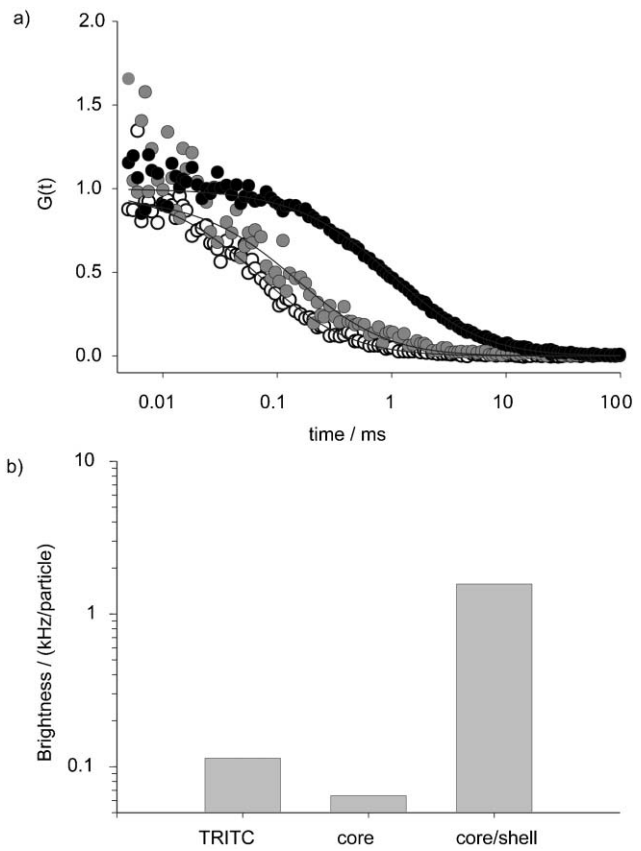

Fig. 4 (a) FCS autocorrelation curves for free TRITC dye (white), TRITC-based silica core particles (grey) and 30 nm core–shell TRITC-based silica nanoparticles (black) and (b) a comparison of per-particle brightness values for TRITC dye, core particles and core–shell nanoparticles. (Reproduced with permission from *Nano Lett.*, 2005, **5**, 113–117.[10] Copyright 2005 American Chemical Society.)

The sequestered, pseudo-solid state environment that the dyes experience within the silica matrix yields a variety of benefits. Beyond the brightness enhancement evident in Fig. 4b, the core–shell architecture prevents the dyes from freely interacting with solvent molecules as indicated in Fig. 5a–b. Free dye molecules exhibit different fluorescent behavior in different solvents (solvatochromic shift) owing to changes in the excited state energies in solvents of different polarity. This is evinced by the $\sim$10 nm blue-shift in absorption and emission peaks for TRITC in ethanol relative to water as shown in Fig. 5a. Once incorporated into the core–shell particles, the same dyes show negligible solvatochromic shifts between the two solvents (Fig. 5b) demonstrating that the dye molecules are effectively removed from interactions with the solvent environment.[10]

In addition to enhanced brightness, narrow size distributions and diminished solvatochromic shifts, encapsulating dyes into the core–shell silica particles also improves their stability against photobleaching. TRITC is inherently a quite stable dye, and thus exhibits less photobleaching than fluorescein, which is commonly used as a photobleaching standard (Fig. 5c). Even so, silica encapsulation reduces TRITC's photobleaching kinetics by approximately an order of magnitude.[19]

Finally, a direct brightness comparison between individual TRITC molecules, optimized C dots encapsulating TRITC and water-soluble quantum dots (CdSe/ZnS) of similar emission wavelength (577 nm) was performed *via* FCS. Within the errors of the measurements, the particle sizes of the C dots and quantum dots were identical (14–15 nm hydrodynamic radius) and measurements were performed on samples of identical optical density. The per-particle brightness values of both C dots and QDs were found to be one to two orders of magnitude greater than free TRITC, while the QDs were only a factor of 2–3 brighter than the C dots (Fig. 5d). These results showed for the first time that organic dye-based probes could be fine-tuned to reach brightness levels similar to quantum dots of the same size in aqueous solution. Subsequent work has shown that the factor of $\sim$30 times increase in brightness of the C dots over free TRITC in water is a result of the product of a per-dye enhancement (see below) and the multiplicity of dye molecules in each particle, implying that the brightness levels may be further increased through optimization of the particle chemistry and architecture.[19]

Quantum dot fluorescence is known to occur primarily by single exciton transitions, while the multiple dye molecules within each C dot absorb and emit independently. This circumvents the issue of stochastic blinking suffered by quantum dots[8] and individual dye molecules under continuous illumination, by providing multiple independent emitters within a single probe. Furthermore, the silica environment not only enhances the fluorescence yield, but also ensures separation between neighboring dye molecules, suppressing energy transfer and quenching. Finally, the silica nanoparticle architecture creates probes that are easier to handle and purify than single dye molecules as well as exposing the silica surface

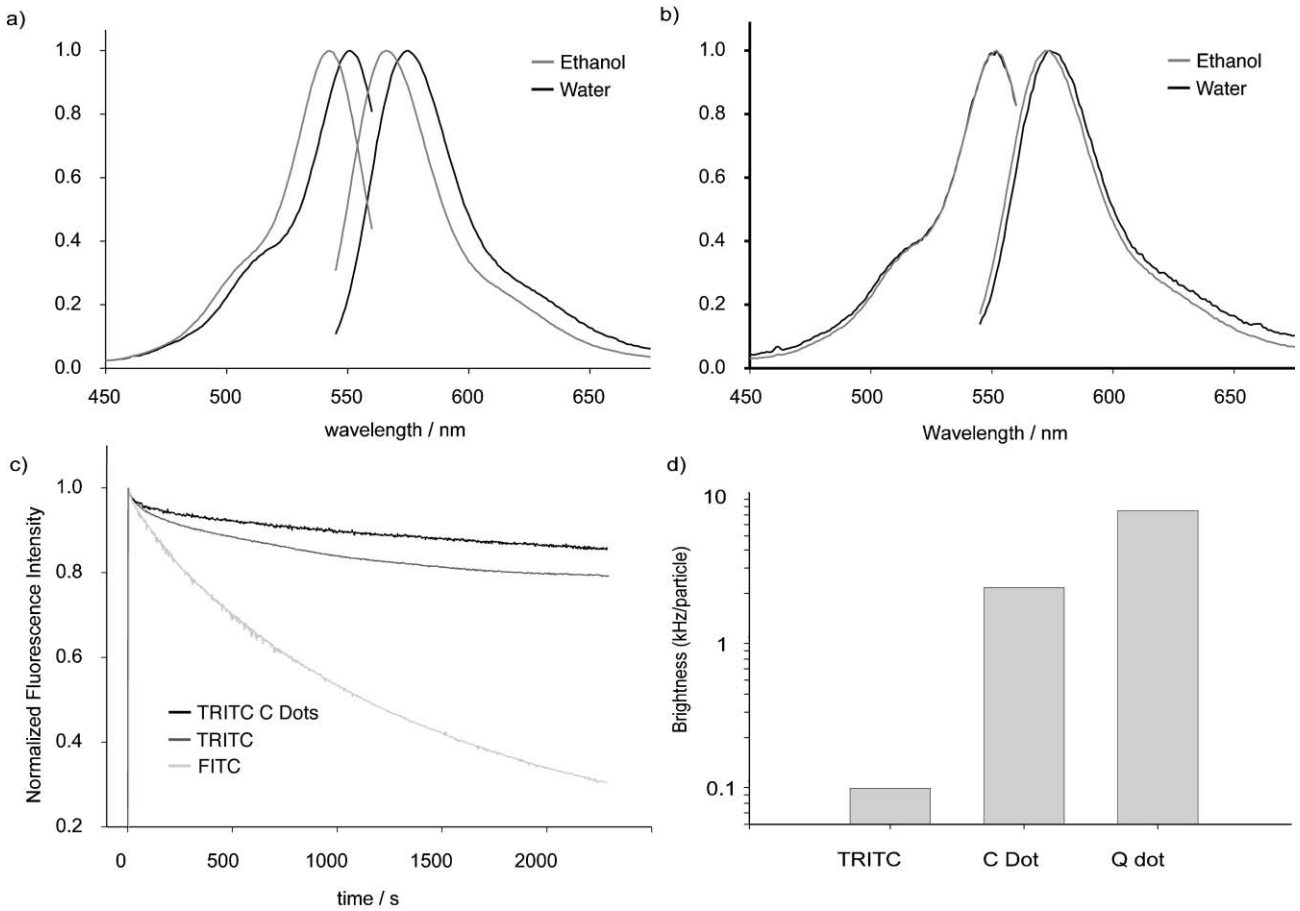

Fig. 5 Absorption and emission spectra for (a) free TRITC dye in water (black) and ethanol (grey) and (b) core–shell TRITC-based silica nanoparticles in water (black) and ethanol (grey) showing the decreased solvatochromic shifts induced by the protective core–shell architecture, (c) Photobleaching measurements of fluorescein (light grey), TRITC free dye (dark grey) and TRITC-based C dots (black) showing the enhanced stability of the core–shell particle architecture, and (d) a comparison of the brightness of free TRITC dye with same-sized C dots and quantum dots in water at the same optical density. (Reproduced with permission from *Nano Lett.*, 2005, **5**, 113–117.[10] Copyright 2005 American Chemical Society).

for conjugation *via* various organosilicates, facilitating multi-functional probes.

2.2 Tuning particle color

To explore the generality of the enhancements of silica encapsulation, we have investigated the behavior of multiple dyes from several dye families throughout the visible spectrum[10,20] as shown in Fig. 6a. As an example, Fig. 6b shows the results of incorporation of 7-nitrobenz-2-oxa-1,3-diazole (NBD) in core–shell silica nanoparticles of similar formulation to those shown above for TRITC.[21] Unlike TRITC, NBD is not optimized for use in aqueous environments, and is known to exhibit low quantum yields ($\sim$0.01) in aqueous solution.[2] For samples of equal optical density (photoabsorption), incorporating NBD in core–shell particles results in significantly increased fluorescence yield relative to unconjugated NBD in water as shown in Fig. 6. It is worth stressing the importance of such emission enhancement for encapsulated dyes as a general concept. Few dyes are optimized for fluorescence in aqueous solution, and those that are tend to be extremely expensive, if at all commercially available. The majority of dyes perform best outside of the aqueous milieu, limiting their applications in biologically relevant fields. Encapsulation of non-optimized organic fluorophores in core–shell silica nanoparticles may render their optical performance in aqueous solution more competitive to highly optimized dyes, opening an area of research that so far has mostly been neglected.

2.3 Tuning particle size

The core–shell architecture can be generalized not only to other dyes and colors, but may also be expanded to cover the gamut of sizes accessible through the Stöber reaction. For applications ranging from biology to photonics, it is desirable to tailor particle size throughout the nanometer to micron scale to study, for example, molecular-scale phenomena in biology or to generate active building blocks for photonic structures. By simply controlling the concentrations of the various reactants in the synthesis, one can tailor the core and shell sizes from nanometers to microns in size as shown in Fig. 7. These scanning electron micrographs depict core–shell TRITC-based fluorescent particles with (a) 50 nm, (b) 150 nm,

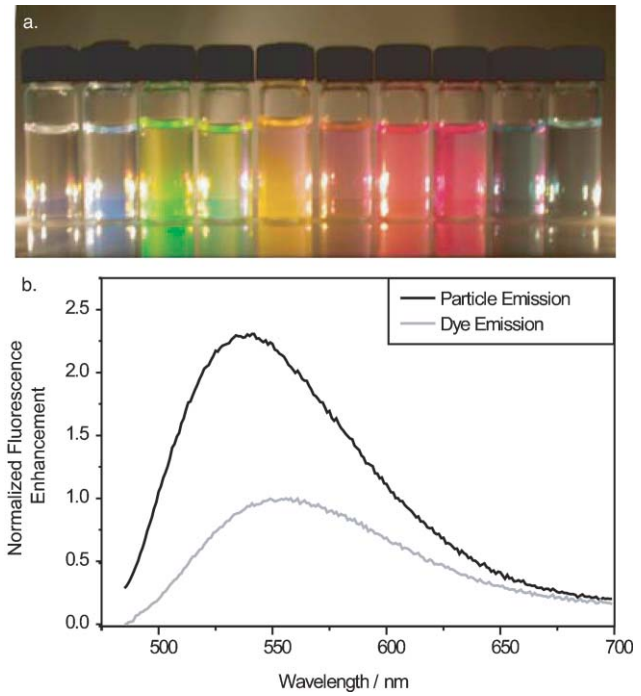

Fig. 6 (a) The core–shell fluorescent silica nanoparticle architecture may be expanded to incorporate a wide range of dye colors by using different dye species in the core including (left to right): AlexaFluor 350, *N*-(7-dimethylamino-4-methylcoumarin-3-yl)maleimide, AlexaFluor 488, fluorescein isothiocyanate, tetramethylrhodamine isothiocyanate, AlexaFluor 555, AlexaFluor 568, Texas Red, AlexaFluor 680 and AlexaFluor 750. (b) Absorption-normalized emission spectra of 7-nitrobenz-2-oxa-1,3-diazole (NBD) free dye (grey) and NBD-based core–shell silica nanoparticles (black), showing greater than twofold enhancement in photoemission for equal peak photoabsorption. (Reproduced, in part, with permission from *Nano Lett.*, 2005, **5**, 113–117.[10] Copyright 2005 American Chemical Society.)

(c) 250 nm, (d) 500 nm, and (e) 1.5 μm diameters. In all cases, the images show the narrow particle size distributions expected from the Stöber synthesis in these size regimes.[13,14,21]

2.4 Tuning collective behavior

The core–shell architecture not only provides a means to engineer the photophysical properties of the encapsulated fluorophores at the single-particle level, but also creates a means to tailor the collective behavior of the particles. For example, in many applications such as thin films, active photonic crystal building-blocks and cellular labeling for

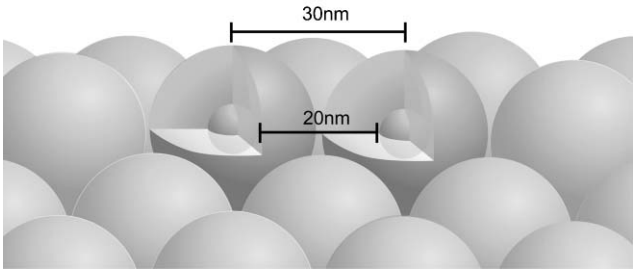

Fig. 8 A schematic illustration of close-packed C dot core–shell silica nanoparticles on a surface, showing the separation of the particle cores, permitting high spatial density of photoemitters without energy transfer between neighboring particles.

confocal microscopy, it is desirable to have extremely dense lateral or three-dimensional packing of emitters to yield maximum brightness. Researchers have tried to create such dense labeling with dye molecules and quantum dots, but often find that these emitters suffer from energy transfer and quenching at high spatial density, counter-acting their high loading.[4]

In contrast, the core–shell architecture allows the fine-tuning of inter-particle interactions by tailoring the shell thickness. Shell thicknesses comparable to the Förster radius of energy transfer[3] preclude interactions between the particle cores and permit dense packing of emitters, creating maximal fluorescence. A simple case of high-density packing is shown in Fig. 8 for particles arrayed on a surface. Each particle core is effectively separated from its neighbors by twice the pure silica shell thickness, creating high spatial emitter density without permitting energy transfer between neighboring fluorophores. As a first example of high emitter density architectures, ultrabright colloidal particles with a raspberry architecture have been produced where the C-dots are deposited as a dense monolayer on ZnS core particles for potential application in active colloidal photonic crystals.[21]

3. Ordered mesoporous fluorescent silica particles

Silica offers a variety of appealing properties as a host material for nanoparticle probes. As a first example towards creating multifunctional particle architectures beyond fluorescence, ordered mesoporosity (2–50 nm) can be integrated through the use of amphiphilic structure-directing agents such as surfactants or block-copolymers. Most of these molecular sieve materials are classified in the M41S family, with the

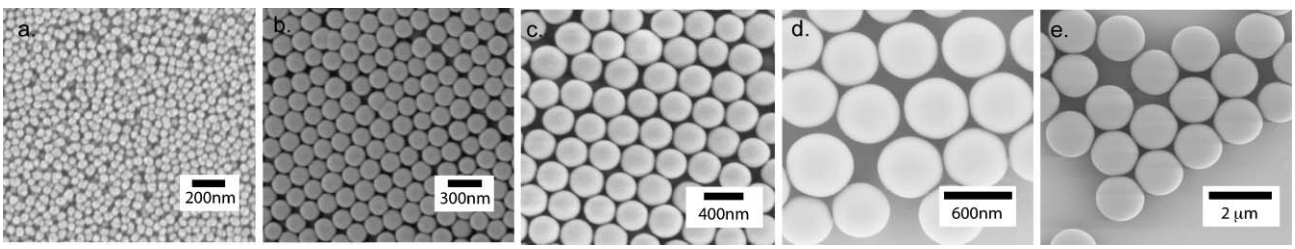

Fig. 7 Representative scanning electron micrographs of core–shell fluorescent silica nanoparticles of different diameters: (a) 50 nm, (b) 150 nm, (c) 250 nm, (d) 500 nm, (e) 1.5 μm.

MCM-41 (hexagonal) and MCM-48 (cubic bicontinuous) classes being most common. The structure and pore size of these materials have been extensively studied since their development at Mobil in the early 1990s,[22] and have attracted much attention for applications in sorption, separation and catalysis as well as within the biological community. MCM-41 (hexagonal) mesoporous materials have been extensively studied as vehicles for controlled therapeutic release,[23] while the biological applications of MCM-48 (cubic bicontinuous) materials are just beginning to be realized.[24] Despite their lack of biodegradability, these silicate materials do offer a variety of interesting attributes including easily tailored pore and particle sizes and facile surface functionalization. MCM-48 materials have even been shown to induce hydroxyapatite growth *in vitro*, making them a potentially viable scaffold for hard tissue (*e.g.*, bone) regeneration.[23]

To explore the use of the MCM-48 materials structure (Fig. 9a) we synthesized fluorescent MCM-48 based silica particles by a modified version of the method of Schumacher *et al.*, using hexadecyltrimethylammonium bromide as the structure-directing agent and integrating covalently-bound TRITC as a fluorescent label.[18,25] The particles were grown to a final diameter of 400 nm (Fig. 9b). Transmission electron microscopy (Fig. 9c) and nitrogen adsorption–desorption measurements (BJH analysis, data not shown) revealed a pore size of 2.74 $\pm$ 0.11 nm, creating particles with large internal surface areas. In order to access all of the internal pores, the templating agent must, of course, be removed. The most complete method of surfactant removal is calcination. This resulted in material with extremely high surface area (BET analysis: 1300 $m^2\ g^{-1}$), but led to sintering of the particles and destroyed the organic fluorophores. Alternatively, repeated washing steps were used to remove the templates. A lower internal surface area of the resulting particles ($\sim$100 $m^2\ g^{-1}$) suggested incomplete template removal, but provided ample volume for initial drug release studies.[18]

In order to assess the viability of the fluorescent MCM-48 particles as a system for cellular uptake and controlled release of, *e.g.*, a drug, we worked with camptothecin, a powerful chemotherapeutic agent, which suffers from low water solubility. The particles were compared with non-porous Stöber-type fluorescent silica particles of a similar size, as well as poly (lactic-co-glycolic acid) (PLGA) polymer-based particles loaded with 15% (w/w) camptothecin (Saltzman Group, Yale University). The mesoporous and non-porous particles were exposed to camptothecin solution in dimethyl sulfoxide (DMSO) and washed thoroughly in phosphate buffered saline solution (PBS) to remove any free camptothecin molecules. Following drug loading, the concentration of camptothecin was quantified in PBS by standardized absorption measurement so that similar drug concentrations could be assessed across different porous host materials. The drug release kinetics were then monitored by spectrophotometry, measuring the optical density of aliquots of the PBS solution at the absorption peak of camptothecin, following the removal of the particles by centrifugation. The data, as plotted in Fig. 9d, show that the silica- and PLGA-based particles exhibit nearly identical drug release behavior, while the non-porous silica particles do not exhibit any appreciable drug release activity. As well, the timescale of release for both the PLGA and MCM-48 are in the clinically relevant realm of hours to days, making them potential candidates for future drug release studies.

It is noteworthy that the PLGA and MCM-48 materials show nearly identical release kinetics, considering that the release mechanisms behind each are quite dissimilar. For PLGA, the entrapped drug molecules are released as the polymer matrix breaks down, while the MCM-48 materials remain intact throughout and slowly release their cargoes by

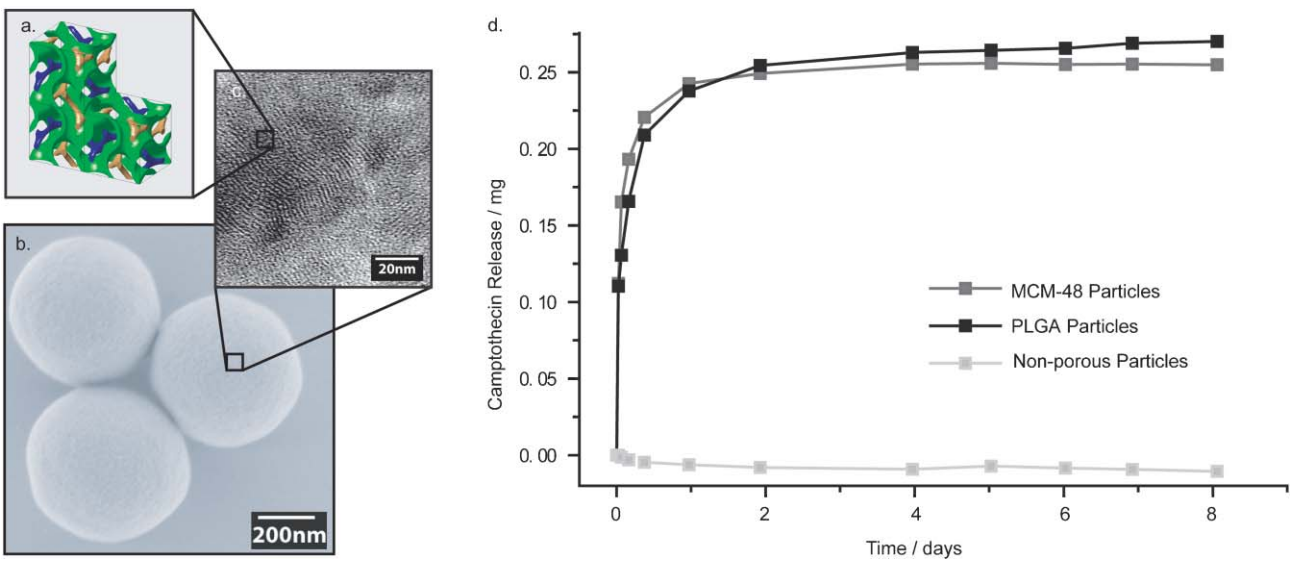

Fig. 9 (a) A structural representation of the MCM-48 cubic bicontinuous porous network; (b) a scanning electron micrograph of 400 nm MCM-48 porous silica nanoparticles; and (c) a thin-section TEM image showing the mesoporous structure of the MCM-type particles. (d) A plot of the drug release characteristics of the MCM-48 nanoparticles (dark grey), PLGA nanoparticles (black) and non-porous Stöber-type nanoparticles (light grey) for the chemotherapeutic agent camptothecin.

diffusion out of the tortuous mesoporous network. This example underscores the versatility of silica as a materials platform for the development of highly functional probes and tools for the life sciences.

4. Colloidal metal nanoshells

Thin metal shells can be grown on the surface of silica nanoparticles to create novel metal/dielectric architectures. Pioneering work in this field was performed by the Halas group, who described the synthesis of gold and silver nanoshells on silica nanoparticles in the 1990s and began to explore the photophysical properties of these new architectures.[26] Colloidal metal shells exhibit plasmon resonances that are tunable over a wide range of frequencies by changing the ratio of core-to-shell thickness. These resonances yield particles that absorb light very strongly at different wavelengths throughout the visible and near-infrared spectrum (Fig. 10).

In these previous works, the metal nanoshells were grown over pure silica nanoparticles bearing no active fluorescent species. It is well known however, that the emission properties of a fluorophore can be dramatically changed by electromagnetic interactions with electron-dense materials such as metals.[27] Further, these interactions can be controlled by altering the geometry of the metal/dielectric system and under favorable conditions can yield benefits such as increased photostability and longer fluorescence lifetimes, without any loss in detectable fluorescence.[27] It is thus interesting to develop C dot-type fluorescent core–shell silica nanoparticles encased in a metal shell, such that the dye–metal shell interactions can be explored though variations in the core–shell/metal–shell particle geometry. To this end, we synthesized C dots encapsulated in a gold shell, shown schematically in Fig. 11a.[18]

These nanoparticles were prepared *via* a step-wise growth of a gold nanoshell around 50 nm C-dot core–shell silica nanoparticles with TRITC-rich particle cores. The gold nanoshell was generated based on the synthetic protocols[26] of the Halas group, wherein nano-sized gold colloids (1.5–3 nm) were attached to the silica particles through silica-bound amine groups. These gold seed particles serve as nucleation points for a homogenous gold shell growth over the particle surface by solution-phase reduction of $HAuCl_4$ by hydroxylamine hydrochloride. In order to produce particles with monodisperse shell thickness and to minimize secondary nucleation of unbound gold particles, the Halas protocols were modified to integrate purification by centrifugation and resuspension between each growth step. Results of this step-wise synthetic procedure are shown in Fig. 11b–e, where the C-dot seed is decorated with 1.5–3 nm gold colloids which grow into a complete metal shell over the course of the three growth steps. Future in-depth photophysical studies can now focus on elucidating the effects of the gold shells on the fluorescence properties of the encapsulated dyes as a function of silica and gold shell thicknesses and overall particle geometry.

In addition, with sufficient excitation power, the metal shell absorptions can be used to dramatically change the local temperature of the environment surrounding the gold nanoshell particles. The Halas and Price groups have recently used this technique to treat tumors within mice. Briefly, gold-coated silica nanoparticles tuned to absorb in the near infrared (820 nm) were injected into a subcutaneous tumor and were subsequently irradiated by a laser. The locations containing gold nanoshell particles increased in temperature by nearly

Fig. 10 Silica-cored gold nanoshell particles of various core–shell thicknesses demonstrating the variety of absorption wavelengths available through fine-tuning the particle geometry. (Reproduced with permission from: ''Nanoshell-Enabled Photonics-Based Imaging and Therapy of Cancer,'' *Technology in Cancer Research and Treatment*, 2004, **3**, 34.[26] Copyright 2004 Adenine Press, http://www.tcrt.org/)

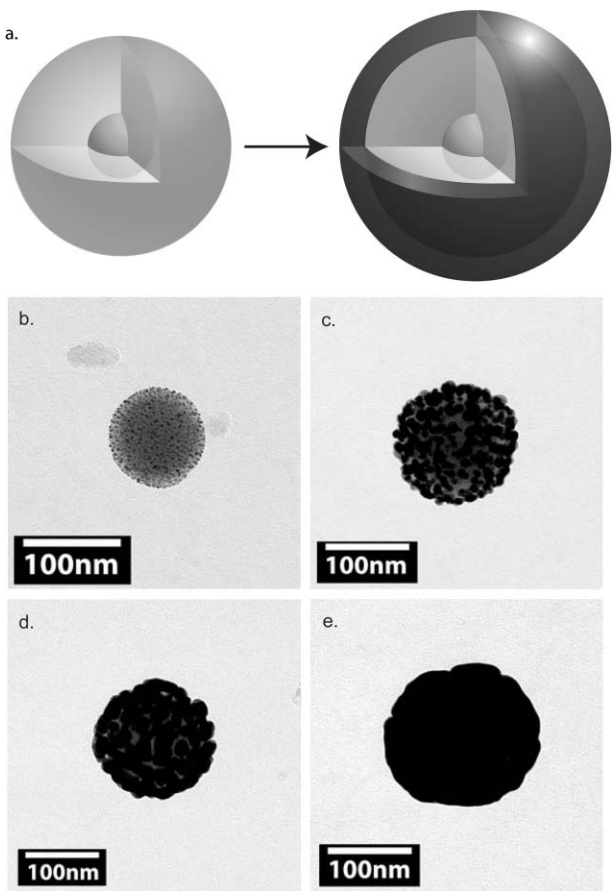

Fig. 11 (a) A schematic depiction of fluorescent core–shell silica nanoparticles encapsulated in a gold nanoshell, and (b–e) representative transmission electron micrographs (TEM) of fluorescent core–shell–gold nanoshell particles grown by step-wise synthesis as described in the text.

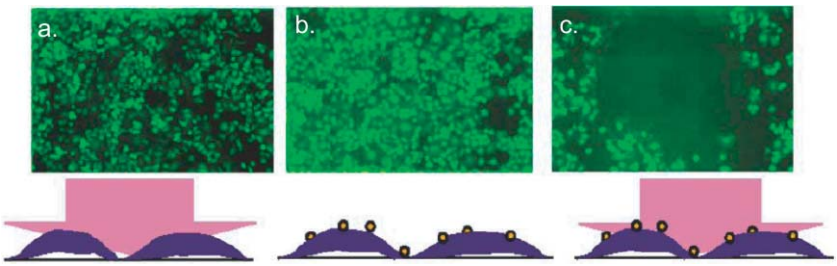

Fig. 12 Fluorescence microscopy imaging of human breast epithelial cells (a) irradiated by 820 nm laser light, (b) exposed to gold nanoshell particles and (c) exposed to gold nanoshell particles and irradiated with 820 nm light. The green fluorescence is calcein green which indicates cell viability. Photothermal exposure in (c) shows localized cell death in the irradiated spot. (Reproduced with permission from: ''Nanoshell-Enabled Photonics-Based Imaging and Therapy of Cancer,'' *Technology in Cancer Research and Treatment*, 2004, **3**, 39.[26] Copyright 2004 Adenine Press, http://www.tcrt.org/)

40 °C, effectively killing the tumor cells, while similarly irradiated areas without particles experienced a non-lethal increase of less than 10 °C (Fig. 12a–c).[26,28]

5. Applications in biology: the field of nanobiotechnology

As demonstrated by this last example, an area of enormous scientific as well as technological promise is the application of nanomaterials in biotechnology and medicine. One of the most powerful paradigms of nanobiotechnology is the design of synthetic materials towards the molecular architecture of biomolecules for enhanced interactions and integration. Indeed, small size and high functionality of materials are keys to understanding the complex interactions in biology on the length scales of proteins, antibodies and organelles, from which future breakthroughs are expected. The combination of enhanced, tunable photophysical properties, variable core–shell architecture, and benign, biocompatible matrix chemistry (silica materials are inert and commonly used in a variety of food and cosmetic products) make C dots an ideal materials platform that can be tailored towards a wide array of applications in the life sciences.

In order to demonstrate the potential of any novel nanoparticle as a fluorescent probe, it is often instructive to use model biological systems. On the cellular level, Rat Basophilic Leukemia mast cells (RBL-2H3) are a robust and versatile cell line and are an excellent candidate for *in vitro* studies with nanomaterials.[29] Mast cells are a class of tissue cells, which are part of the first line of immunological defense in vertebrates. These cells are integral to the immune response to environmental stimuli such as allergens and bacteria, and are known to express cell-surface receptors for antibodies such as Immunoglobulin E (IgE). Upon IgE-binding and cross-linking, mast cells undergo a transformation from their resting state (Fig. 13a) to an activated state (Fig. 13b) with concomitant release of signaling molecules such as histamine, which mediate the allergic response throughout the body. The RBL-2H3 cells are a continuously-cultured cell line commonly used in studies of allergic response because they are easily sensitized towards various stimuli.[29] They will be employed as the biological model system in the remainder of this review.

5.1 Integrating imaging with targeting: C-dot antibody conjugates

One of the desirable features of a biological probe is that it can be targeted to a specific biological environment with minimal non-specific labeling. Surface functionalization of silica is well established and may be performed with an array of biologically active substances from small molecules to antibodies to create such probes. Indeed, various groups have demonstrated the use of antibodies, peptides and small molecules to mediate biological recognition.[12] An example of this concept for TRITC-based C dots was demonstrated through antibody-mediated labeling of cell surface receptors on RBL cells. Specifically, the work investigated the interaction between IgE antibodies and the FcεRI cell surface receptor. FcεRI is integral to the cell's response to foreign materials in the bloodstream and is known to form a strong, but reversible complex with IgE both *in vivo* and *in vitro*.[30] Upon exposure to an allergen, IgE antibodies specific to that allergen bind to and cross-link the FcεRI cell surface receptors. This initiates a signal cascade throughout the cell, ultimately leading to degranulation and release of histamine and heparin, the latter of which transduces further steps in the allergic response, which can eventually cause allergy symptoms throughout the body and thus a systematic response at the macroscopic length scale.[29]

For these experiments, 30 nm diameter TRITC-based C dots were exposed to the IgE antibodies and allowed to bind *via* adsorption to the silica surface. These particle–antibody

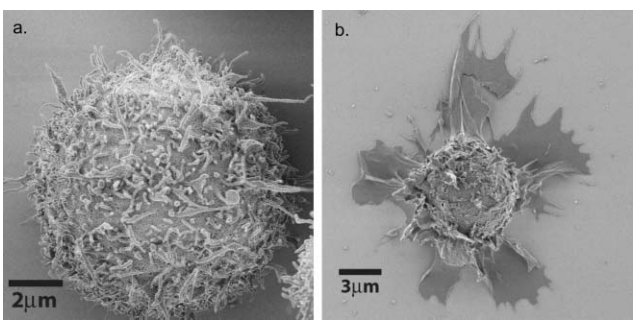

Fig. 13 Scanning electron micrographs of fixed Rat Basophilic Leukemia (RBL) mast cells in their (a) resting and (b) excited states.

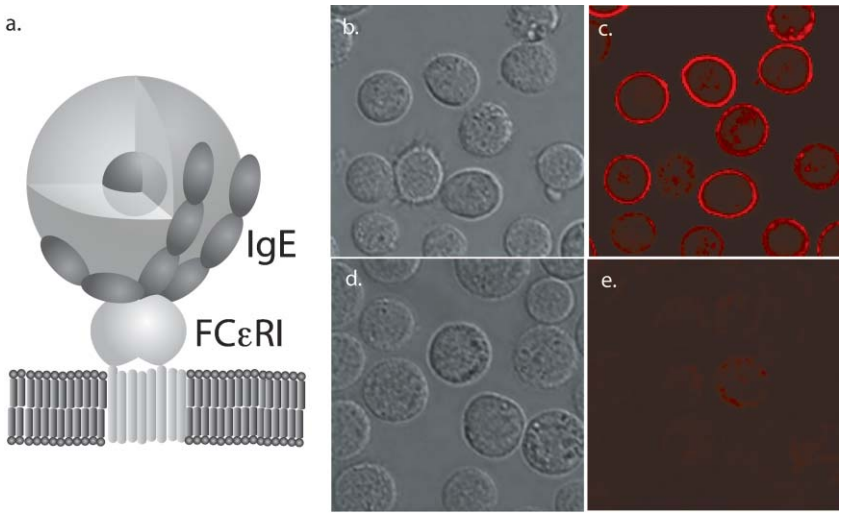

Fig. 14 A schematic illustration of a fluorescent core–shell silica nanoparticle non-covalently attached to an Immunoglobulin E (IgE) antibody specifically attached to the FcεR1 cell surface receptor of an RBL cell, and (b) brightfield and (c) confocal fluorescence images of RBL cells with IgE-mediated cell surface labeling. As a control (d) brightfield and (e) fluorescence images of RBL cells quenched with free IgE after exposure to C dot–antibody complexes showing minimal non-specific cell surface binding.

complexes were then incubated with RBL cells. It was found that they specifically attached to the cell surface *via* the IgE–FcεRI interaction schematically depicted in Fig. 14a. Representative results are shown as brightfield and confocal fluorescence images in Fig. 14b–c, demonstrating equatorial labeling of the cell membranes by the nanoparticle–antibody complexes. The images reveal even labeling levels across the whole cell membrane. As a control, cells were incubated with free IgE antibodies to quench the FcεRI receptors before incubation with the C dot–IgE complexes under the same conditions as above. These experiments revealed no appreciable cell surface binding after washing, as shown in the bright field and confocal fluorescence images in Fig. 14d–e.[10] The combination of specific targeting and the robust nature of these core–shell fluorescent silica nanoparticles creates an ideal tool for long-term studies such as determining the fate of antibodies or other proteins in a variety of biological systems.

5.2 Integrating imaging with sensing: C dot sensors

The final example of a highly functional core–shell architecture involves the development of C dot sensors for near-molecular scale chemical sensing, building on the bright and stable C dot platform to create environmentally-sensitive probes.[31] On the cellular and sub-cellular level, chemical gradients are crucial to the communication and function of living systems. The concentrations of ions such as Na^+, Ca^{2+} and H^+ are very closely controlled in both space and time, and changes in these concentrations can be indicative of such cellular activities as neural/muscular signaling, vesicle trafficking, or more broadly, overall cellular health. For example, within eukaryotic cells, materials (*e.g.* drugs, proteins) that are endocytosed by the cell are transported through a series of membrane-bound organelles known as endosomes, which transport their cargo throughout the cell. In many cases, materials that are taken up by the cell go through a series of membrane-bound vesicles with sequentially lower pH until reaching the lysosome where the foreign material is ultimately degraded in a low pH environment.[32] On a slightly larger scale, the rapid growth of tumor cells often outstrips the available blood supply, yielding an acidic and hypoxic environment within the growing tumor.[33] Thus, the ability to quantitatively image the concentrations of biologically active ions, such as H^+, are of major importance in understanding metabolic processes in both *in vitro* and *in vivo* experiments.

Ion concentrations such as pH are traditionally analyzed by macroscopic means, such as titration or probes such as litmus paper or electrochemical cells. These approaches lack the small size and spatial/temporal resolution to effectively probe ion concentrations within cells or tissues. Thus, a variety of approaches to nanoscale sensing have been developed which rely on analyte-specific effects on the wavelength, lifetime or quantum yield of fluorophore emission. The smallest assays are analyte-sensitive dyes, such as fluorescein (pH sensor) and Fluo-4 (Ca^{+2} sensor).[2] However, the vast majority of these molecular sensors can only provide qualitative data, as the measured fluorescence intensity is dependent not only on the analyte concentration, but also on the concentration of the sensor.[34] Additionally, like all free dye molecules, they are limited in brightness and are prone to photobleaching, cellular toxicity and solvatochromic shifts.[3]

To address these issues, several groups have begun developing particle-based hybrid systems incorporating a second dye species to create an internal standard, which allows the analyte concentration to be determined independent of the sensor concentration by analyzing the ratio between the two signals. This so-called ratiometric sensing enables quantitative chemical sensing down to the single nanoparticle level. Among the variations on this concept are polymer-based sensors, lipid vesicle-based sensors and silica-based sensors. Polymer-based sensors are currently the most common, including commercially-available dextran-based pH sensors[2] and the larger PEBBLE sensors developed by the Kopelman group.[35] The

PEBBLE sensors integrate sensor and reference dye molecules homogenously into a single cross-linked polymer particle. Although these particles integrate multiple dye molecules to increase individual probes' brightness, like all polymer-based probes, the dyes are given relatively little protection against quenching and leaching. Another approach, pursued by the Rosenzweig group, is the use of supported lipid bilayer vesicles as vehicles for the reference and sensor dyes. These microparticles provide a highly biocompatible alternative to polymers, though they lack the robustness and small size to effectively probe intracellular conditions.[36] To address some of these issues, the Kopelman group recently developed homogeneously-dyed ratiometric nanoparticle sensors for dissolved oxygen based on sol–gel silica[37] which provides a more robust vehicle for the sensor dyes.

The optimized core–shell sensor architecture. The core–shell C dot architecture is ideally suited to the development of ratiometric fluorescent sensors on the nanoscale (Fig. 15). By placing the internal reference dyes in the sequestered particle core environment, they are protected from external influences such as solvent and other large molecules, providing a stable reference signal. The sensor dyes can then be integrated covalently into the particle shell, protecting the reference dyes. Further, this arrangement affords the sensor dyes the benefits of attachment to the silica matrix, while exposing the sensors on the highest surface-area portion of the particle. This provides greater sensitivity and more uniform response than particles with sensor and reference dye molecules dispersed homogeneously throughout the particle. As well, covalent attachment of both sensor and reference dyes minimizes dye leaching to create stable sensors with low background signal.

As proof-of-principle for this dual-emission core–shell sensor nanoparticle architecture, the Wiesner group developed a ratiometric pH sensor for quantitative *in vitro* chemical imaging and spectrofluorometric analysis.[31] Fluorescein isothiocyanate (FITC) was chosen as a pH sensor dye for its significant change in quantum yield upon protonation/deprotonation of the hydroxyl groups on the xanthene backbone of the dye. In the protonated, mono-anionic form, the dye exhibits a relatively low quantum yield of 36%, whereas upon deprotonation the quantum yield increases to 93% for the dianion form.[2] With a pK_a of 6.4, this transition makes fluorescein an excellent sensor for pH in the biologically

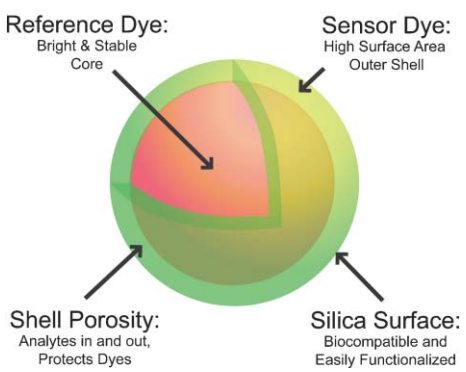

Fig. 15 A schematic illustration of the dual-emission core–shell nanoparticle sensor architecture highlighting several design advantages.

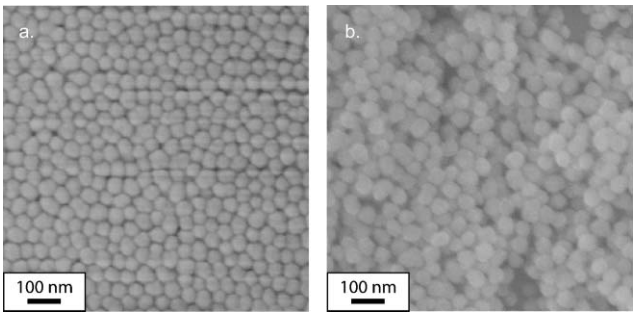

Fig. 16 Scanning electron microscopy images of (a) 50 nm TRITC-based core particles and (b) 70 nm dual-emission pH sensor nanoparticles incorporating fluorescein isothiocyanate as a sensor dye and TRITC as a reference dye. (Reproduced with permission from *Small*, 2006, **2**(1), 723–726.[31] Copyright 2006 Wiley VCH.)

relevant range from pH 5–8.5. TRITC was chosen as the internal standard because its quantum yield is unaffected by pH changes in this realm. The TRITC-containing core particles were grown to 50 nm in size *via* a modified Stöber reaction, as shown in the scanning electron micrograph in Fig. 16a. FITC-based fluorescent silica precursors were synthesized and integrated into a 10 nm thick shell layer around the TRITC cores to yield 70 nm core–shell sensor particles as shown in the SEM image in Fig. 16b. In both cases, monodisperse particles with smooth and uniform surfaces were produced. This particle size and architecture was chosen for ease of uptake into cells[38] as well as ease of handling during synthesis and characterization.

The pH-dependent spectra of the particles were analyzed by spectrofluorometry (Fig. 17a). The ratio between the peak emission intensities of the sensor and reference dyes were calculated for particles in a variety of pH-calibrated phosphate buffer solutions (pH 5–8.5) and were plotted *versus* pH (Fig. 17b). The resulting calibration curve exhibits the typical behavior of a system in equilibrium between two states, in this case the mono- and di-anionic protonation states of fluorescein with a pK_a at pH 6.4, which is in accordance with literature.[2] The particles were similarly analyzed on a confocal fluorescence microscope to develop a calibration curve for ratiometric imaging of pH.

Intracellular ratiometric pH imaging. An important goal of nanoparticle sensors is the ability to perform quantitative chemical measurements inside individual cells facilitating spatial and temporal mapping of metabolic parameters within the cell. To demonstrate the C dot sensor's capabilities, RBL mast cells were again chosen as a model system for their particle-uptake characteristics and several interesting pH-related biological questions that remain under investigation. Initial experiments were performed with single-emission TRITC core–shell particles of the same core–shell geometry as the sensors, which showed that the RBL mast cells do not naturally uptake 70 nm particles (Fig. 18a). However, upon addition of phorbol 12,13-dibutyrate (PDB) the particles were rapidly endocytosed into various intracellular vesicles (Fig. 18b). PDB is a commonly used reagent in DNA transfection experiments and it is thought to stimulate

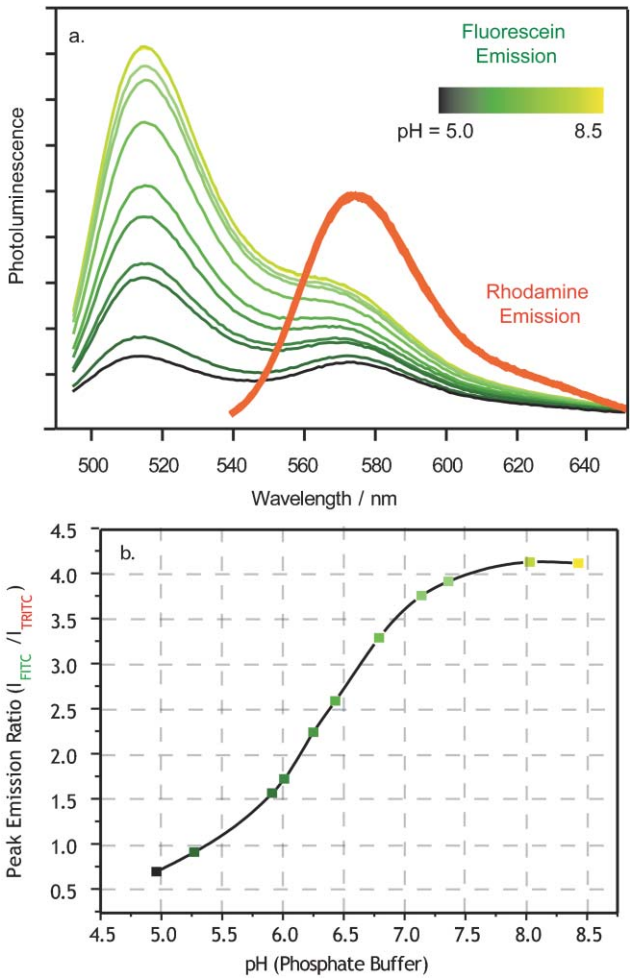

Fig. 17 (a) Spectrofluorometry data for 70 nm dual-emission core–shell fluorescent silica nanoparticle pH sensors showing fluorescein (green) and TRITC (red) in phosphate pH calibration buffers from pH 5–8.5. (b) A ratiometric calibration curve based on the peak intensity ratio between fluorescein and TRITC across the pH range under investigation. (Reproduced, in part, with permission from *Small*, 2006, **2**(1), 723–726.[31] Copyright 2006, Wiley VCH.)

macropinocytosis and concomitant uptake of membrane-associated and extracellular material.[39]

The same uptake protocols were then followed for the dual-emission sensor particles that were readily endocytosed as well. Following uptake, the particles were trafficked into early endosomal compartments, which sort incoming material to various intracellular destinations. For the sensor nanoparticles, these early endosomes matured into late endosomes and eventually lysosomal compartments with much lower pH. This progression was imaged *via* confocal fluorescence microscopy as shown in Fig. 19. The reference and sensor channels were imaged using separate excitation to avoid spectral bleed-through as shown in Fig. 19a–b. The reference dye (TRITC) channel acts not only as an internal standard for pH measurements but also as an indication of particle location and local concentration allowing the particles to be tracked throughout the cell (Fig. 19a). The ratio between the sensor (Fig. 19b) and reference emission channels was calculated for each pixel and using the previously determined calibration

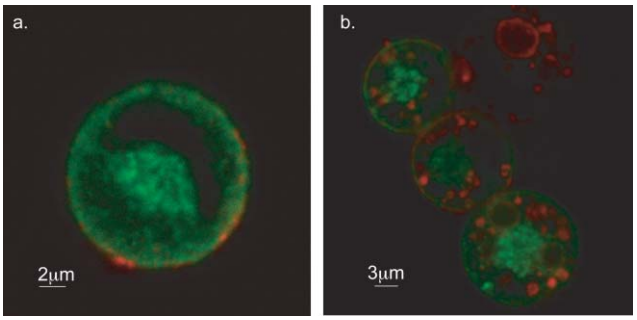

Fig. 18 (a) 70 nm single-emission sensor particle analogs (red) incubated with RBL mast cells (green) and (b) 70 nm single-emission sensor particle analogs (red) in intracellular vesicles following exposure to phorbol dibutryate. (Reproduced with permission from *Small*, 2006, **2**(1), 723–726.[31] Copyright 2006 Wiley VCH.)

curve, the corresponding pH values were represented in the false-spectrum image shown overlaid on a transmitted-light image of the cell in Fig. 19c. Various intracellular locations reveal pH values varying from ~pH 6.5 (early endosome) to

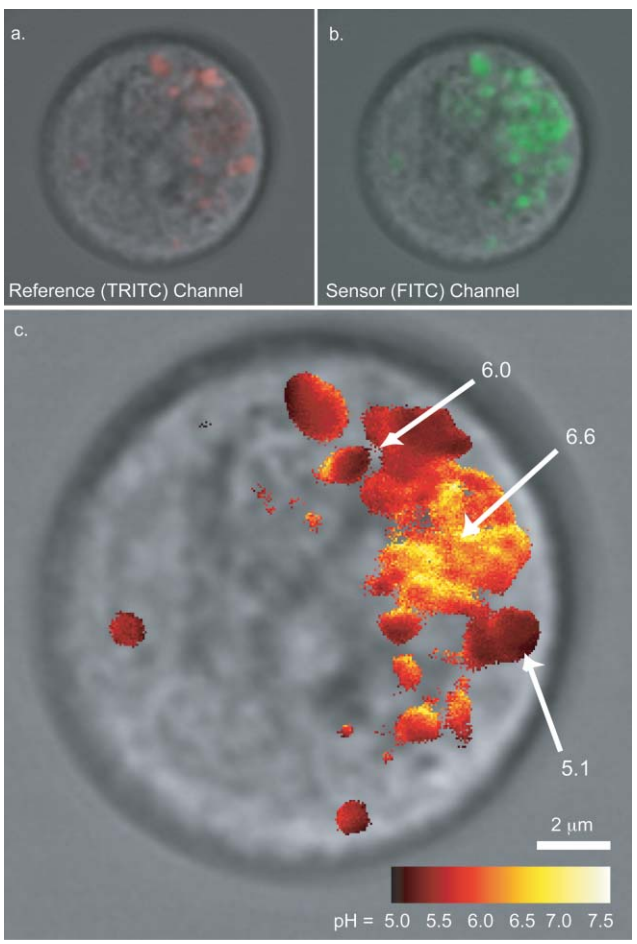

Fig. 19 Confocal fluorescence images of (a) red reference dye (TRITC) emission, (b) green sensor dye (fluorescein) emission as well as (c) quantitative ratiometric confocal imaging of pH within an RBL mast cell, all overlaid on brightfield cell images. (Reproduced, in part, with permission from *Small*, 2006, **2**(1), 723–726.[31] Copyright 2006 Wiley VCH.)

late endosomal and lysosomal compartments with much lower pH values between 5–5.5. These results demonstrate the applicability of the concept of dual-emission core–shell silica sensor nanoparticles for investigating fundamental biology at the molecular level and open the door to further experiments building upon the specific targeting capabilities of these nanoparticles to investigate biological phenomena.

This sensor architecture may be of particular importance in complex biological environments where many species can potentially interfere with sensing. Since many fluorophores with sensing capabilities are available, this approach may be generalized towards multiple analytes, including metal ions, oxygen, or redox status indicators. Cocktails of such particles may further allow high content imaging for high throughput drug screening whereby metabolic parameters of cells are monitored with high temporal and spatial resolution down to the molecular level.

6. Conclusions: highly integrated particles—towards "Lab on a Particle" architectures and single particle laboratories

Throughout this review, a variety of functionalities have been introduced that demonstrate the versatility of silica as a host material for fluorescent dyes for many applications, specifically in the fields of nanobiotechnology and the life sciences. The power of silica as a host material is twofold. First, encapsulation of organic dyes in a silica matrix can enhance their stability and performance (*e.g.* brightness). Second, the ability to synthesize particles with core–shell architectures allows multiple functions to be brought together in a single vehicle, separated in different shells, for example, to minimize interference towards creating highly functional particles.

The first of these two points reveals an interesting aspect of nanotechnology, *i.e.* the ability to improve an existing technology through the application of small-scale structures and materials. As discussed in the first section of this review, organic dye molecules have been investigated for decades. Highly optimized, water-soluble organic dyes have been developed and are now commercially available for prices per weight much higher than that of gold. Enhancing the performance of dyes through encapsulation in water soluble core–shell silica nanoparticles may significantly reduce costs and at the same time catapult performance characteristics of relatively inexpensive dyes to competitive levels.

The fluorescent core–shell silica nanoparticle design concepts exemplified by the sensors introduced in the last section hint at the possibilities available to researchers in the future. By combining such functionalities as antibody-mediated targeting, mesoporosity and chemical sensing already demonstrated individually, a "single-particle laboratory" or "lab on a particle" can be envisioned that would, for example, (a) seek out a specific cellular location, (b) deliver a payload of therapeutics and (c) subsequently monitor the cell's response. These particles would provide high-content feedback on the activity of the therapeutic agent, rather than simply monitoring whether or not the cells survived treatment, as is commonly the case today.

Many other such combinations can be envisioned, with more functionalities such as enzymatic catalysis or magnetism, that can be easily integrated. With the development of these and other functionalities, one can envision a "toolbox" of capabilities, which can be assembled in different shells to create probes tailored to explore specific biological questions at near-molecular scale. The versatility of silica as a host material and the modularity of the core–shell architecture thus provide a wide and open space for innovative research towards creating highly-integrated and highly-functional nanomaterials for nanobiotechnology and beyond.

Acknowledgements

This review is based on several years of research on fluorescent silica nanomaterials performed at Cornell University. We would like to thank the following collaborators for their contributions to the research: Tara Zedayko, Daniel Bonner, Katherine Chin and Erik Herz for particle synthesis; Daniel Larson and Watt Webb for photophysical characterization; Mamta Srivastava, Prabuddha Sengupta and Barbara Baird for cellular application of the particles; Mark Saltzman for drug release studies; and Carol Bayles and Malcolm Thomas for their oversight on confocal fluorescence and scanning electron microscopy, respectively. Funding for this research included grants from the Cornell Center for Materials Research (CCMR—NSF MRSEC DMR 0520404), the National Science Foundation (NSF—NSF grants: NIRT 0404195, DBI-0080792), Phillip Morris USA and the Cornell Nanobiotechnology Center (NBTC—STC Agreement No. ECS-9876771). Finally, we would like to thank Gil Toombes for rendering the MCM-48 structures shown in this review as well as Erik Herz for fruitful discussions and careful reading of the manuscript.

References

1 F. Wang, W. Tan, Y. Zhang, X. Fan and M. Wang, *Nanotechnology*, 2006, **17**, R1–R13(and references therein).
2 R. P. Haugland, *The Handbook – A Guide to Fluorescent Probes and Labeling Technologies*, Molecular Probes, Eugene, OR, 10th edn, 2005.
3 J. R. Lakowicz, *Principles of Fluorescence Spectroscopy*, Kluwer Academic, New York, 2nd edn, 1999.
4 T. Maka, S. G. Romanov, M. Muller, R. Zentel and C. S. Torres, *Phys. Status Solidi B*, 1999, **215**, 307–312.
5 R. Tsien, *Annu. Rev. Biochem.*, 1998, **67**, 509–544.
6 I. Medintz, H. Uyeda, E. Goldman and H. Mattoussi, *Nat. Mater.*, 2005, **4**, 435–446.
7 A. M. Derfus, W. C. W. Chan and S. N. Bhatia, *Nano Lett.*, 2004, **4**, 11–18.
8 J. Yao, D. Larson, H. Vishwasrao, W. Zipfel and W. Webb, *Proc. Natl. Acad. Sci. U. S. A.*, 2005, **102**, 14284–14289.
9 T. Pellegrino, S. Kudera, T. Liedl, A. Javier, L. Manna and W. Parak, *Small*, 2005, **1**, 48–63.
10 H. Ow, D. Larson, M. Srivastava, B. Baird, W. Webb and U. Wiesner, *Nano Lett.*, 2005, **5**, 113–117.
11 F. J. Arriagada and K. Osseo-Asare, *J. Colloid Interface Sci.*, 1995, **170**, 8–17.
12 L. Wang, K. Wang, S. Santra, X. Zhao, L. Hilliard, J. Smith, Y. Wu and W. Tan, *Anal. Chem.*, 2006, 646–654.
13 W. Stöber, A. Fink and E. Bohn, *J. Colloid Interface Sci.*, 1968, **26**, 62–69.
14 G. H. Bogush, M. A. Tracy and C. F. Zukoski, *J. Non-Cryst. Solids*, 1988, **104**, 95–106.

15 A. van Blaaderen and A. Vrij, *J. Colloid Interface Sci.*, 1993, **156**, 1–18.
16 S. Hess, S. Huang, A. Heikal and W. W. Webb, *Biochemistry*, 2002, **41**, 697–705.
17 W. Zipfel, R. Williams and W. W. Webb, *Nat. Biotechnol.*, 2003, **21**, 1369–1377.
18 H. Ow, Ph.D. Thesis, Cornell University, 2005.
19 D. Larson, H. Ow, W. Webb and U. Wiesner, in preparation.
20 E. Herz, D. Bonner and U. Wiesner, in preparation.
21 E. Herz, A. Burns, S. Lee, P. Sengupta, D. Bonner, H. Ow, C. Liddell, B. Baird and U. Wiesner, *Proc. of SPIE*, 2006, **6096**, 609605.
22 C. T. Kresge, M. E. Leonowicz, W. J. Roth, J. C. Vartuli and J. S. Beck, *Nature*, 1991, **359**, 710–712.
23 M. Vallet-Regi, L. Ruiz-Gonzalez, I. Izquierdo-Barba and J. Gonzalez-Calbet, *J. Mater. Chem.*, 2006, **16**, 26–31.
24 Y.-S. Lin, C.-P. Tsai, H.-Y. Huang, C.-T. Kuo, Y. Hung, D.-M. Huang, Y.-C. Chen and C.-Y. Mou, *Chem. Mater.*, 2005, **17**, 4570–4573.
25 K. Schumacher, P. Ravikovitch, A. Du Chesne, A. Neimark and K. Unger, *Langmuir*, 2000, **16**, 4648–4654.
26 C. Loo, A. Lin, L. Hirsch, M.-H. Lee, J. Barton, N. Halas, J. West and R. Drezek, *Technol. Cancer Res. Treat.*, 2004, **3**, 33–40 and references therein.
27 J. Enderlein, *Appl. Phys. Lett.*, 2002, **80**, 315–317.
28 J. Hirsch, R. Stafford, J. Bankson, S. Sershen, B. Riviera, R. Price, J. Hazle, N. Halas and J. West, *Proc. Natl. Acad. Sci. U. S. A.*, 2003, **100**, 13549–13554.
29 D. Holowka and B. Baird, *Annu. Rev. Biophys. Biomol. Struct.*, 1996, **25**, 79–112.
30 P. Schwille, U. Haupts, S. Maiti and W. W. Webb, *Biophys. J.*, 1999, **77**, 2251–2265.
31 A. Burns, P. Sengupta, T. Zedayko, B. Baird and U. Wiesner, *Small*, 2006, **2**, 723–726.
32 H. Lodish, A. Berk, S. Zipursky, P. Matsudaira, D. Baltimore and J. Darnell, *Molecular Cell Biology*, W. H. Freeman, New York, 4th edn, 1999.
33 P. Carmeliet and R. Jain, *Nature*, 2000, **407**, 249–257.
34 Z. Gryczynski, I. Gryczynski and J. R. Lakowicz, *Methods Enzymol.*, 2003, **360**, 44–75.
35 S. M. Buck, Y.-E. L. Koo, E. Park, H. Xu, M. A. Philbert, M. A. Brasuel and R. Kopelman, *Curr. Opin. Chem. Biol.*, 2004, **8**, 540–546.
36 A. Ma and Z. Rosenzweig, *Anal. Bioanal. Chem.*, 2005, **382**, 28–36.
37 H. Xu, J. W. Aylott, R. Kopelman, T. J. Miller and M. A. Philbert, *Anal. Chem.*, 2001, **73**, 4124–4133.
38 W. Zauner, N. Farrow and A. Haines, *J. Controlled Release*, 2001, **71**, 39–51.
39 C. Ra, K. Furuichi, J. Riviera, J. Mullins, C. Isersky and K. White, *Eur. J. Immunol.*, 1989, **19**, 1771–1777.

